Characterization of Rust Layers on Weathering Steels Air-Exposed for a Long Period *

Katsuhiko Asami and Michio Kikuchi

Institute for Materials Research, Tohoku Univesity, Sendai 980-8577, Japan

Several weathering steels and a plain carbon steel exposed to atmosphere for 17 years at Yokkaichi (at a coastal and industrial region) and Mikuni Pass (at a rural region) in Japan were analyzed and compared to find effects of environments on the formed rusts. Specimens were examined with electron probe microanalysis (EPMA), X-ray diffraction (XRD) and transmission electron microscope (TEM). Their cross-sections were also analyzed by EPMA. XRD detected mainly α-FeOOH as major rust constituent and β-FeOOH and γ-FeOOH as minor ones in the surface region. The concentration of β-FeOOH was especially high on the skyward surface of all the specimens irrespective of steel composition. EPMA results showed that Si, Na, S were abundant on the skyward surface. In the cross-section, alloying elements Cu and Cr were enriched in the inner layer of rust as well as Si, while P and Ni did not show any characteristic distribution. TEM examination of cross-section of rusts showed that α-FeOOH was also main constituent of the rust. The β-FeOOH showed no special distribution feature in the main part of rust except in the very surface region. Amorphous rust judged from electron diffraction pattern and Fe_3O_4 distributed mainly near the interface between steel and rust layer. The γ-FeOOH was contained much more in rust on plain carbon steel than weathering steels. A quantity ratio α/γ^*, that is, the ratio of α-FeOOH to the sum of β-FeOOH, γ-FeOOH and magnetite, is >1 for a weathering steel, and <1 for a mild steel. The Si in the inner layer was suggested in the form of SiO_4^{4-} state. There was almost no difference between specimens exposed at the industrial region and the rural region because of chloride sprayed for melting snow on road during winter at the rural region.

1. Introduction

Recently, importance of low-alloy weathering steels is more increasing for the reason that those steels can be applied to large structures such as bridges without painting, and hence their low maintenance cost. Especially, when they were used for bridges without painting under mild environments, the results are actually satisfying. However, the origins of their protective nature even under mild atmosphere have not been clarified yet. There are also various arguments about the formation conditions of the protective rust layer on weathering steels, and it is not solved fully yet. Okada *et al.*[1] studied the rust layer produced by air exposure for several years, and surmised that the dense and compact amorphous oxide layer in an inner layer where Cu and P were enriched would bear corrosion resistance. Misawa *et al.*[2,3] have analyzed the steels exposed to air for 26 years at the industrial area, and reported that the γ-FeOOH which had been formed at early stage changed to amorphous rust, which changed to α-FeOOH further, and that Cr was enriched in the iron oxyhydroxide, α-FeOOH. By the transmission electron microscope (TEM), Yamamoto *et al.*[4] observed the rust layer of weathering steels exposed to air at the rural area for 35 years and found that the amorphous and the crystalline portions were intermingled in the inner layer of the rust layer. Shiotani *et al.*[5] analyzed the rust layer formed on the 27 years old weathering steel bridge exposed in coastal industrial zone, and reported that γ-FeOOH and β-FeOOH existed in an outer layer and amorphous rust in the inner layer, and that α-FeOOH spread in the wide range of the inner rust layer. They also reported that Cr, Ni and Cu was enriched in the inner layer, and Cu

concentrated both at the crack of the inner rust layer and in pits of the steel. Furthermore, Kihira[6] claimed that the cation selectivity of a rust layer was important for improvement of protectiveness of the rust layer. Keiser *et al.*[7] found out δ-FeOOH from the rust layer of the steel exposed for several years in the industrial area, and reported coexistence of about ten% of γ-FeOOH and a small amount of α-FeOOH.

Thus, it is hard to say that recognition of the rust layer is obtained commonly. Consequently, it is the first importance to characterize the rust layer on the weathering steels in detail. Recently, an paper was published where the results on the properties and functions of protective rust layers formed on weathering steels exposed to air for 17 years in various parts of Japan was reported.[8] Here in this study, the rust layers formed on steels exposed at an coastal industrial region and at a rural region were characterized in detail by X-ray diffraction (XRD), electron probe microanalysis (EPMA), scanning electron microscopy (SEM) and transmission electron microscopy (TEM), and the results were compared each other to find effects of environments on the formed rusts.

2. Experimental

Four types of weathering steels and a plain carbon steel were exposed to air for 17 years from 1981 to 1998. Exposure sites were Yokkaichi on Route 23 (a coastal industrial region, Site No. = 19) and Mikuni Pass on Route 17 (a rural region, Site No. = 08), in Japan. Details of steels used for experiments are listed in Table 1 including their chemical analysis data. Average deposition rates of air-born chloride ions and sulfate ions were listed in Table 2 where environmental data were measured in 1990. The deposition rate of Cl^- is expressed in the weight of NaCl assuming all Cl^- is

---

Table 1 Chemical compositions of steels.

Steel	Steel type	Chemical composition (mass%)										
		C	Si	Mn	P	S	Cu	Cr	Ni	Nb	Ti	V
A	SM50	0.17	0.32	1.39	0.016	0.012	—	—	—	—	—	—
B	SMA50AW	0.12	0.39	0.90	0.008	0.006	0.36	0.61	0.22	0.014	—	—
C	SMA50AW	0.11	0.20	0.68	0.014	0.010	0.30	0.51	0.13	—	—	—
D	P–Cu–Cr–Ni	0.06	0.36	1.26	0.091	0.006	0.34	0.35	0.30	—	0.015	0.05
E	P–Cu	0.06	0.53	1.42	0.085	0.004	0.32	—	0.02	0.02	—	—

Table 2 Environments of the exposure sites.

Site No.	Bridge	Exposure location	Deposition rate of Cl^-, $gNaCl \cdot m^{-2} \cdot s^{-1}$	Concentration of sulfurous acid Gas, $gSO_3 \cdot m^{-2} \cdot s^{-1}$	Distance from coastline, km
08	Oominezawa bridge	Mikuni Pass, Gumma Pref. Rural region	1.04×10^{-8}	1.16×10^{-9}	155.0
19	Yokkaichi overhead bridge	Yokkaichi, Industrial region	9.49×10^{-8}	12.6×10^{-9}	1.6

in the form of NaCl. Similarly, the deposition of sulfur is expressed in the weight of SO_3. Steel coupons were placed horizontally on weathering test racks under bridges at respective sites. Accordingly, the measurements for the skyward face "A" were distinguished from those for the earthward face "B" because skyward faces can not be equal to the earthward faces from the environmental point of view. Notation of specimens was expressed by a combination of steel name, exposure site number, facing direction (all "horizontal" in this report), and specimen face (skyward or earthward). For example, A19H-B corresponds to a specimen of "Steel A" exposed at Site "19", with its face parallel to the ground (horizontal), "H", and the earthward side face "B". Rusts on skyward and earthward surfaces of specimens were examined by EPMA (JEOL JXA-8621MX) and XRD (Rigaku Rotaflex RU-200B with a rotary Cu target and monochromator of pyrolytic graphite; $\lambda = 0.15148$ nm for Cu Kα) without removing the rusts from the steels after the surfaces were just cleaned with water, but the loose components such as loose rust on surfaces were removed, which spalled off easily from the surface of the steels during handling and specimen preparation. XRD measurement was carried out by glancing angle incidence XRD method ($\alpha - 2\theta$ method) where the X-ray incidence angle α was fixed to 10°. For EPMA measurements, a wave length dispersive X-ray spectrometer was used. The electron acceleration voltage was 20 kV and the incident electron beam current was 50 nA. Pentaerythritol (PET) crystal was used for measurements of P, S, Cl, K, Ca, Ti, Cr and Mn, thallium acid phthalate (TAP) crystal for Na, Mg, Al and Si, and lithium fluoride (LIF) crystal for Fe, Ni, Cu and Zn. Quantitative analysis was carried out by a standardless method with ZAF (atomic number, absorption, fluorescence) matrix correction using intensities of K$_\alpha$ lines of all the detected elements in rust layer except oxygen, and the data were normalized to 100%. Quantitative and ZAF correction softwares used in this experiment were XM-86PACWE and XM-86PACZAF, respectively, which were installed to the EPMA apparatus. A mean value of a set of data at different five positions on the same surface of a specimen was taken as an EPMA analysis re-

sult. Composition of the rust layer from the surface to about 1 μm deep was obtained by EPMA measurements from the surface. For compositions at deeper regions in the rust layer, the cross-section was also analyzed by EPMA. Cross-section of a specimen was obtained by embedding the specimen in resin followed by cutting it. The cross-section was finished by polishing with silicon carbide paper followed by diamond paste polishing. Thickness of rust layer was estimated from the cross-section images of the rust layer observed by SEM. The elemental distribution in the cross-section was also quantitatively measured by EPMA. Two-dimensional distribution of major elements for a region of 200 μm or 250 μm square was first measured by mapping method, and the data was converted to depth profiles by summing up all the counts parallel to the steel surface. For quantitative estimation of the mapping data, the background was subtracted. The EPMA measurements were done at the position where the thickness of rust layer was largest or the most corroded region within the cross-section of 3 cm. Rust constituents in the rust layer were determined by TEM and electron diffraction (ED) for the plain carbon steel specimens (A19H-A and A19H-B) and weathering steel specimens (E19H-A, E19H-B) exposure to air in Yokkaichi. The proportion and distribution of α-FeOOH, β-FeOOH, γ-FeOOH, magnetite, and amorphous rust were estimated from TEM observation. Here, amorphous rust was judged from electron diffraction pattern. TEM specimen were prepared by ion-milling of the thinly sliced cross-section of rust layer. Observation was done at the thin portion around a hole where the electron beam can pass through. By controlling the size of a hole, it was possible to observe the whole range of the rust layer from the surface to the interface between the rust layer and the steel. Observation was done at 20–30 points for each specimen.

3. Results and Discussion

3.1 XRD and EPMA results of rust layer surfaces

There is no clear difference between the XRD pattern of rust layers formed on a plain carbon steel and those on weath-

ering steels. However, there was clear difference between the XRD patterns of the skyward surfaces and those of earthward surfaces. The averaged XRD patterns of the skyward surfaces of all the specimens and that of earthward surface of all specimens are compared in Fig. 1, where XRD patterns of the standard substances, α-FeOOH and β-FeOOH are also plotted. In Fig. 1, the differential diffraction pattern between the skyward and earthward surfaces is also shown. The main difference in XRD pattern between the skyward and earthward surfaces appeared between $2\theta = 30°$ and $40°$ where the patterns obtained from earthward surfaces had two strong peaks while the rust layer on skyward surfaces had only one strong peak. As can be seen clearly in the figure, the main constituent is α-FeOOH in both the skyward and earthward surfaces, and, in addition, β-FeOOH and γ-FeOOH also exist although the pattern of the standard γ-FeOOH XRD pattern is not shown here. There is apparent difference between the XRD patterns of skyward and earthward surfaces. By comparing with the standard XRD patterns, it can be understood that the differential pattern between the skyward and earthward surfaces correspond to β-FeOOH, that is, all specimens contain much β-FeOOH on the skyward surfaces. It can be said that the concentration of β-FeOOH was especially high on all the specimens irrespective of steel composition. The same results were obtained for specimens exposed at Site 08, Mikuni Pass. Magnetite was not detected on both surfaces. Because the incident angle of the X-ray was fixed to 10°, the depth of the rust layer where diffraction signal comes from is limited to *ca.* 1.2 μm under the assumption of a completely flat surface.[9] The sampling depth by XRD will be much less than the total rust layer thickness although there is remarkable unevenness in the sample surface. The results shown in Fig. 1 are, therefore, the results of the rust layer in the range of 2–3 μm from the top surface at maximum. It can be said that the results are just for the surface region of the rust layer. It means these results does not deny the existence of magnetite underneath. The rust layer in deeper region should be containing different species from those in the surface region observed by XRD.

The average concentrations of main elements detected by EPMA on the surface regions of the rust layer are shown in Figs. 2(a) and (b) for specimens exposed at Site 08 (Mikuni Pass) and Site 19 (Yokkaichi), respectively. The concentrations in Fig. 2 are those normalized to 100 at% for all the elements detected except oxygen, and they are also averaged for all steels. At Mikuni Passs (Site 08), Cl and Ca are remarkably concentrated on skyward surface in comparison to the earthward surface, suggesting they are coming down as big drops rather than aerosol. If chloride ion had come as aerosol, it should have deposited on both side equally. The concentration of Na is very low in comparison with Cl while that of Ca is comparable to Cl at Site 08 indicating the origin of Cl is calcium chloride rather than NaCl. It is well known that calcium chloride is used for melting snow on road during winter. Actually, there is a large amount of snow fall in the region of Site 08 during winter. Probably, data shown in Table 2 did not take the chloride sprayed on road during winter into the Cl⁻ deposit measurement. On the other hand, the data at Yokkaichi (Site 19) shown in Fig. 2(b), concentration of Na is almost equal to that of Cl indicating its origin is NaCl. Actually, the distance from the ocean to Site 19 is only 1.6 km as shown in Table 2. Moreover, NaCl should be very fine particles or aerosol because both Na and Cl appear almost equally on both the earthward and skyward surfaces.
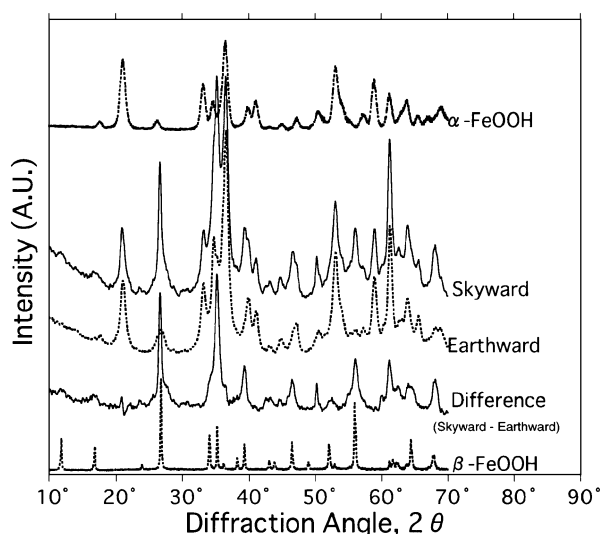

Fig. 1   X-ray diffraction pattern of the skyward and earthward of rusted specimens exposed at Yokkaichi (Site 19) and their difference together with standard patterns of α-FeOOH and β-FeOOH.
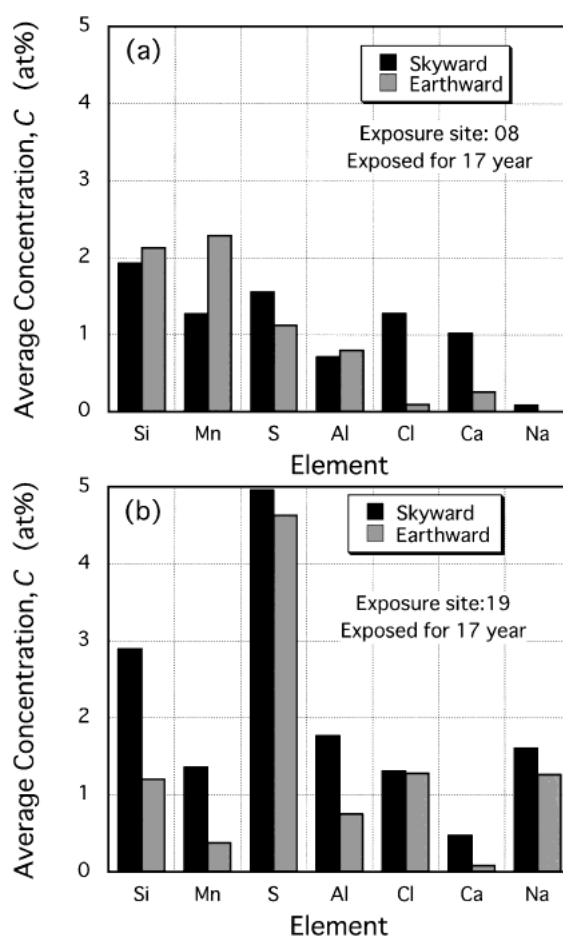

Fig. 2   EPMA results of the rusts on the skyward and earthward surfaces of steels exposed at (a) Mikuni Pass (Site 08) and (b) Yokkaichi (Site 19) for 17 years.

Concentrations of S on specimens exposed at Site 19 are about 4–5 fold of that at Site 08. It is reasonable because the SO_3 concentration in air at Site 19 is very high as shown in Table 2. However, the concentration of S measured on specimens at Site 08 is also high in comparison with the SO_3 concentration in air as shown in Table 2. The concentration of S at Site 08 can not be realized from the SO_3 concentration in air. Its origin is, therefore, unable to be attributed to SO_3 gas in air. It can be derived from MnS in steels since concentrations of Mn and S are approximately equal on specimens exposed at Site 08.

Nickel and chromium were found only on steels which contain them as alloying elements. On specimens exposed at Site 08, Cu was detected only on few specimens. On the other hand, on all the Cu-containing specimens exposed at Site 19, Cu was detected.

3.2 Observation of cross section of rust layers

An example of SEM image of cross section of specimen is shown in Fig. 3. It can be seen that corrosion proceeds deeply in part but it does not develop at another place, and accordingly the thickness of rust layer is also changing with places. The rust layer thickness appeared in Fig. 3 does not correspond to real corrosion depth because the loose rust layer on surfaces had been removed when cross section was prepared. The average corrosion rate of a plain carbon steel (Steel A) at the coastal industrial region was 4.2×10^{-13} m·s^{-1}, and that of a weathering steel (Steel B) was 3.0×10^{-13} m·s^{-1}, and those values at Site 08 were reported as 1.3×10^{-13} m·s^{-1} and 0.93×10^{-13} m·s^{-1}, respectively.[10] The ratio of corrosion rates of Steel A to Steel B can be calculated as about 1.4 at both the coastal industrial region and the rural mountainous region. The maximum thickness of the rust layer of Steel A at the rural mountainous region is 165 μm, and 115 μm for Steel B; that is, thickness ratio is 1.44, which is almost equal to the ratio of the corrosion rates. At the coastal industrial region, the thickness of the rust layer on Steel A is 142 μm, and that on Steel B is 150 μm. It results in the ratio of rust layer thickness 0.95, indicating that the rust layer on Steel A (a plain carbon steel) easily spalled off from the surface, and the measured thickness of the rust layer on Steel A appeared thin whereas that on Steel B did not exfoliated because of high adhesiveness.

3.3 EPMA results of rust layer cross sections

In order to examine distribution of elements in rust layers, cross sections of specimens were measured by EPMA. Mapping of elements were first measured and the results were
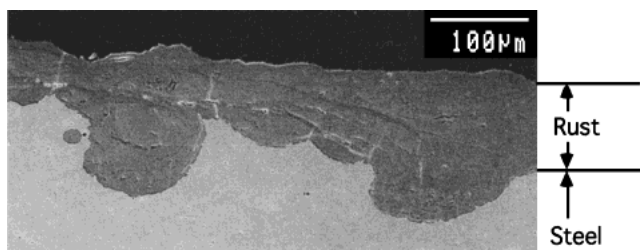
converted to quantitative depth profiles. For conversion from mapping data into depth profiles, background counts were removed. By removal of background counts, the accuracy of the quantitative measurements was markedly improved. The results are shown in Figs. 4–7.

In general, a rust layer consists of inner and outer layers, and Si, Cu and Cr distribute in the inner layer. On the other hand, P and Ni are uniformly distributed over the whole layer although they are slightly more in the inner layer. Manganese is more in the outer layer. On the skyward rust layer of Steel A (a plain carbon steel), Cl and S distribute mainly in the outer layer, and Na in the inner layer, but it is not clear on the earthward rust layer. On the weathering steel specimen D19H, Cl and Na situate in the outer layer; Na especially is in the outer layer, but S does not show a clear deviation of distribution. Figures 4–7 show results at the coastal industrial region, Yokkaichi. It is essentially the same when exposed at the Mikuni Pass, a rural mountainous region. Moreover, almost the same results were obtained for the other steels shown in Table 1.

The structure of rust layer is typically shown in Fig. 8 based on the above observation and the analysis of the rust layer surface. In Fig. 8, the distribution of the detected elements except Fe, O, Ni and P is shown. It is well known that Ni and P are important elements which impart protective function to the weathering steel. But they are omitted in the figure because their distribution is rather flat and do not show enrichment in a special layer. Rust consists of three layers fundamentally,

Fig. 3 SEM image of the cross section of skyward side of a weathering steel (E19H-A) exposed at Yokkaichi (Site 19) for 17 years.
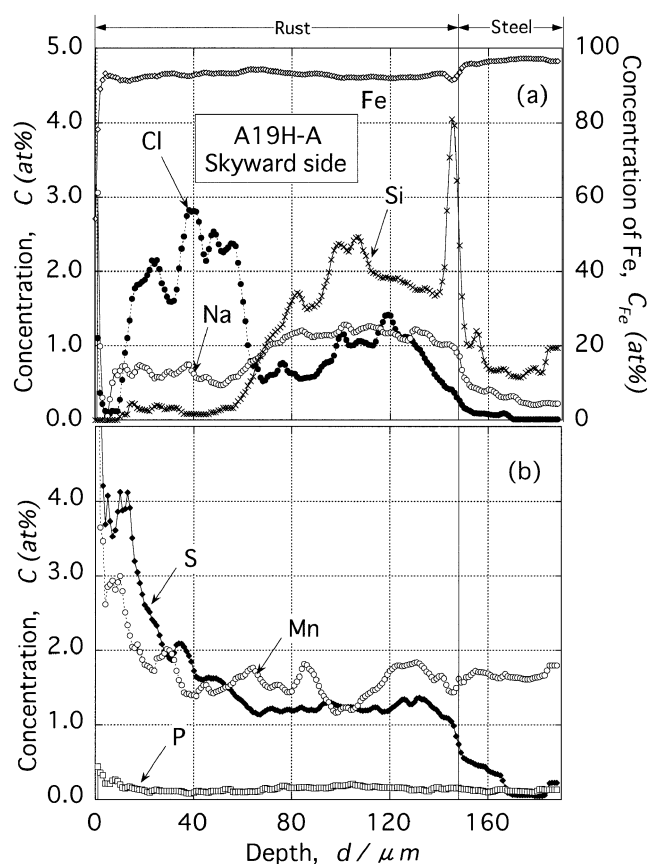

Fig. 4 Depth profiles of (a) Fe, Si, Na, Cl and (b) S, Mn and P in the rust on the skyward side of a mild steel specimen (A19H-A) exposed at Yokkaichi (Site 19) for 17 years.
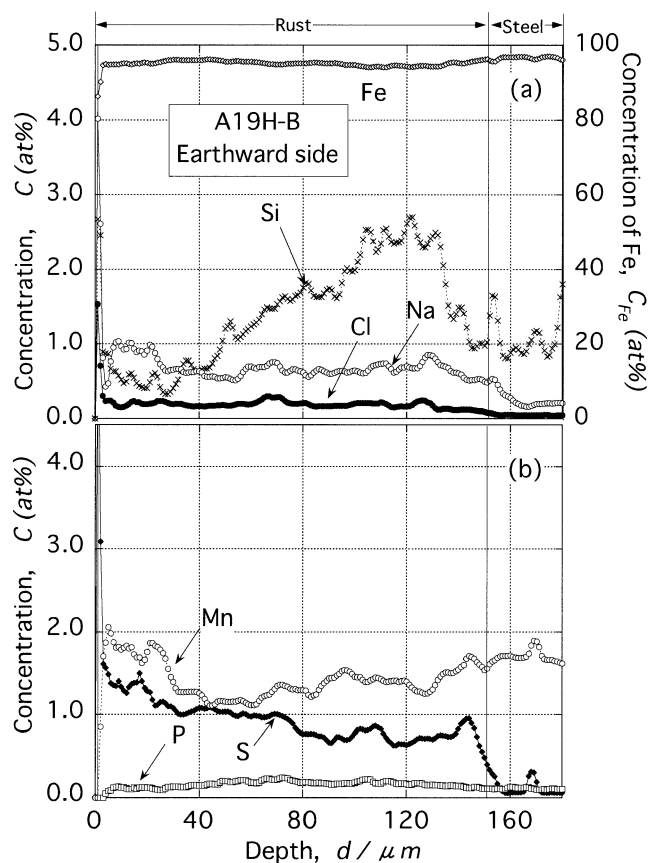
Fig. 5   Depth profiles of (a) Fe, Si, Na, Cl and (b) S, Mn and P in the rust on the earthward side of a mild steel specimen (A19H-B) exposed at Yokkaichi (Site 19) for 17 years.
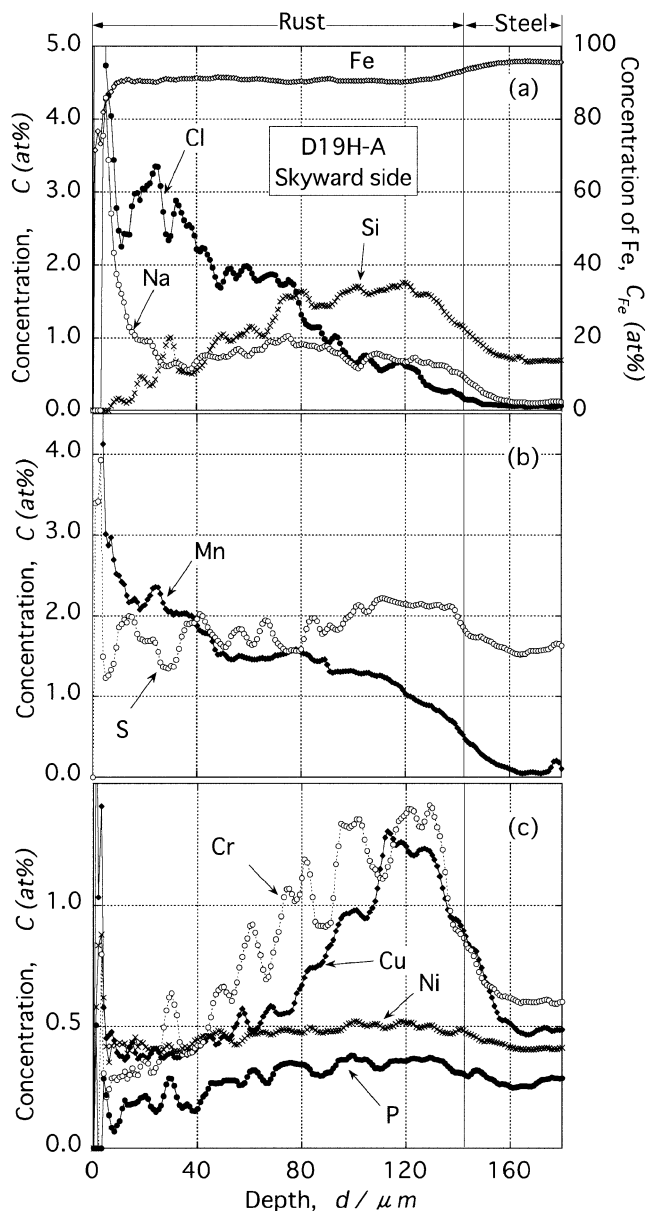

Fig. 6   Depth profiles of (a) Fe, Si, Na, Cl, (b) S, Mn and (c) Cr, Cu, Ni and P in the rust on the skyward side of a weathering steel specimen (D19H-A) exposed at Yokkaichi (Site 19) for 17 years.

the outermost layer with a thickness of 3 μm or less, an outer layer, and an inner layer. The thicknesses of an outer layer and an inner layer depend on steels, sides (skyward side or earthward side) and the environment of the exposure sites. Thickness of inner layer seemed not sensitive to the side of surface, that is, there is no large difference between the skyward and earthward surfaces. The thickness of outer layer is, however, dependent on side; the thickness is smaller on the earthward side surface than the skyward side surface.

Concentration of Mn is generally high in the outer layer. In steels, manganese exists as MnS particles. When the concentration of SO_2 is low in the exposure environment, the most of S in the rust layer comes from MnS in steels. However, distributions of Mn and S in the rust layer are not in accordance because MnS react with air easily and form stable substances in the rust layer. Sulfer in the rust layer comes also from the environment when the concentration of SO_2 is high in environment.

It was reported that the corrosion loss of weathering steels at Yokkaichi (Site 19) was in general about twice that of Mikuni Pass (Site 08).[10] However, both specimens do not show such a difference in the rust layer thickness obtained from cross-sectional observation. Rust on weathering steels is compact, and difficult to exfoliate. This characteristic will contribute to the protective property. Okada et al.[1] reported that a large quantity of amorphous rust were formed because of Cu and P were condensed in the inner layer within the rust layer, which could impart protective property to the weather-

ing steels. However, the enrichment of P in the inner layer was not observed in this report, and the relation of P and amorphous rust was not clear, either. Misawa et al.[2,3] studied Cr-containing steels and found that α-FeOOH in which Cr was partly substituted for Fe had much higher protectiveness than conventional α-FeOOH. It was made clear in this work that not only Cr but also Cu and Si are enriched in the inner rust layer as shown in Figs. 4–7. According to Sakashita and Sato,[11] the ion selectivity of rust has an important role for the protectiveness of rust; i.e., oxyhydroxides in general has anion selectivity, but that it changes to cation selective when some anions such as phosphate and molybdate ions adsorbed. This means that if the rust layer formed on a weathering steel is cation selective, the penetration of anions such as Cl^- will be hindered, and the rust layer will be protective against corrosion. If elements enriched in the inner layer can impart cation selectivity to the rust layer, the rust layer formed on
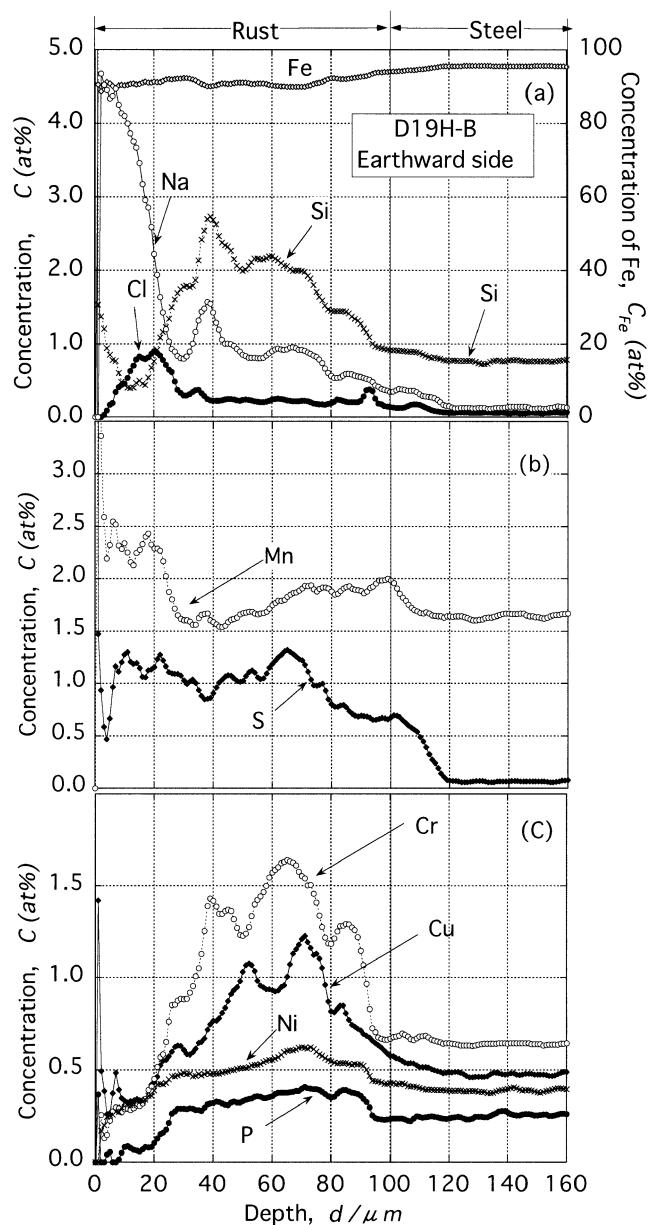
Fig. 7 Depth profiles of (a) Fe, Si, Na, Cl, (b) S, Mn and (c) Cr, Cu, Ni and P in the rust on the earthward side of a weathering steel specimen (D19H-B) exposed at Yokkaichi (Site 19) for 17 years.

Fig. 8 Rust structure on a weathering steel estimated from EPMA measurements.

Fig. 9 Si K_β spectrum of Si in the rust on specimen E19H-A together with those of pure silicon, $NaAlSi_2O_6$, SiO_2 and Fe_2SiO_4.

the steels will be protective. Yamashita et al.[12] reported that Cr(III) was substituted for Fe(III), cation selectivity increased certainly. However, effect of Si which is also enriched in the inner layer was not mentioned.

In order to make the role of Si clear, the chemical state of Si in the rust layer was estimated by measuring Si K_β X-ray spectrum. In Fig. 9, Si K_β spectrum from the rust layer of E19H-A is shown. For comparison, Si K_β spectra of several standard substances, pure Si, $NaAlSiO_6$, SiO_2 and Fe_2SiO_4 are also measured and shown in Fig. 9. By comparison with the Si K_β spectra of standard substances, it can be said that the spectrum of E19H-A is most close to Fe_2SiO_4; pure Si shows a peak at a clearly different position, and it is also different from the spectra of $NaAlSiO_6$ and SiO_2. It is, therefore, most probable that most of Si in the inner rust layer is in the form of iron silicate. Similarly, Si in the rust layer on A19H-A showed a peak at the same position. It can be said that the Si
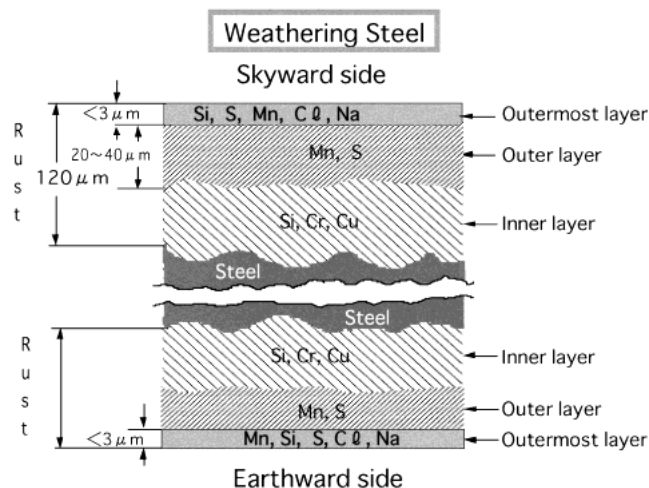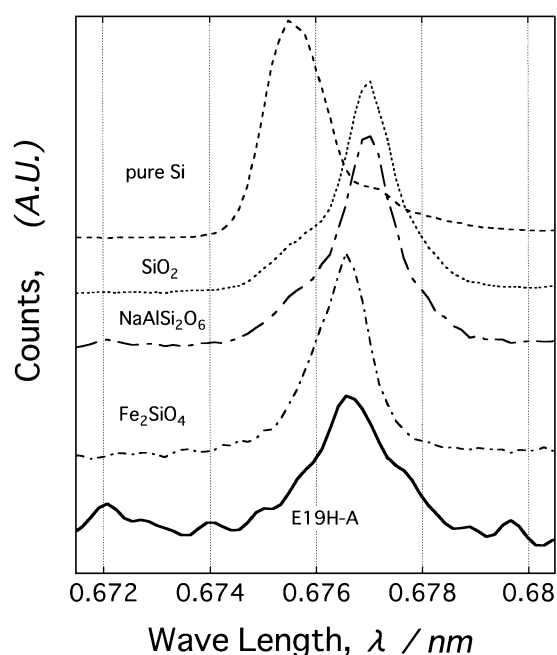
in the rust layer comes from steels rather than the deposition from outside. However, its role is not known yet, and more examination will be required about the role of the Si in the rust layer.

3.4 Results of TEM and ED analyses

For specimens A19H-A, A19H-B, E19H-A and E19H-B, distribution and abundance of α-FeOOH, β-FeOOH, γ-FeOOH, amorphous rust and magnetite in a rust layer were investigated using TEM and ED. Examples of TEM images of rust and their diffraction patterns are shown in Figs. 10(a) and (b). The former and the latter correspond to regions where α-FeOOH and β-FeOOH are exclusively observed, respectively. Other than the five components listed above, a rust expressed by $(FeOOH)_3 \cdot (Fe_2O_3)_4$ was found, but it was found to be an artifact during specimen preparation for TEM. α-FeOOH consists of fine crystallites. It can be observed that
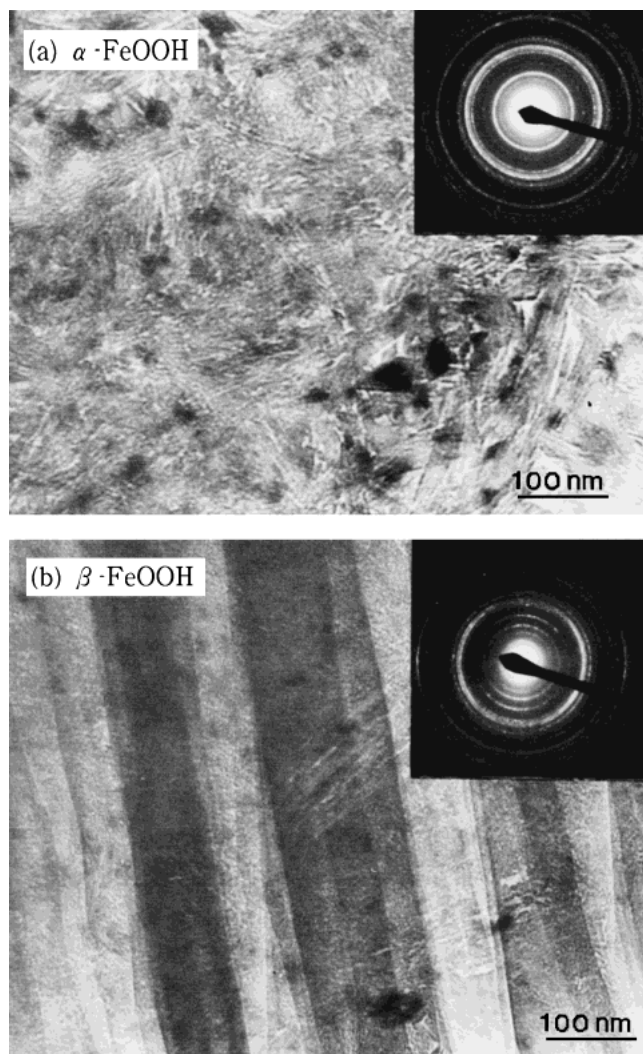
Fig. 10   Typical bright field images and electron diffraction patterns from a rust layer on a corroded steel: (a) α-FeOOH and (b) β-FeOOH.

Fig. 11   Percentage among crystalline rust components on skyward side and earthward side of a mild steel (A19H) and a weathering steel (E19H).

their grain sizes are several nm and more, and it is very fine fiberous structure. They are intricately entangled. On the other hand, β-FeOOH is beltlike shaped with several nm in width and several μm in length; the length can not be seen in the figure. Since beltlike crystallites are gathered well ordered, it turns out that ED shows strength distribution peculiar to fiber structure.

Among rust constituents, α-FeOOH was the main constituent in all specimens. The distribution of β-FeOOH was not regularly distrbuted, but it was rather abundant at outer region. On a plain carbon steel specimen (A19H-A), amorphous rust and magnetite were abundant at the bottom of the rust layer. The clear boundary between the inner layer and outer layer observed by EPMA was not observed by TEM/ED. It might be caused the fact that the distribution of constituents of rust layer was judged only from observation of a certain specific domain along the edge of a hole made with ion milling technique. Future examination is required much more on the distribution of rust constituents.

The average abundance of α-FeOOH, β-FeOOH, γ-FeOOH, and magnetite in the rust layer formed on a plain carbon steel (A19H) and a weathering steel (E19H) after air exposure for 17 years in Yokkaichi was estimated semi-
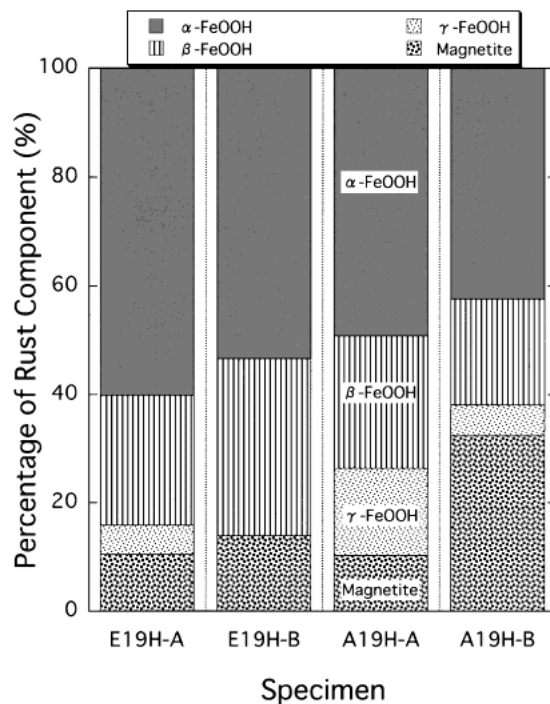
quantitatively from the relative electron diffraction intensity belonging to respective components at each observation. Within the present experiment, the correlation between abundance of amorphous rust and steel materials or exposure side (skyward or earthward) was not clear. In general, it is difficult to quantify amorphous rust from electron diffraction intensities. Especially quantification of amorphous species should cause large uncertainty. In Fig. 11, abundance among only crystalline rusts in the rust layer is shown. In the same way as the results of X-ray diffraction of the rust layer from the surface, it is clear that the α-FeOOH is the main constituent in rust layer on a plain carbon steel (A19H) and on a weathering steel (E19H). Magnetite appears more on earthward side than skyward side, and more on Steel A than Steel E, while γ-FeOOH is more abundant on skyward side than earthward side. Moreover, γ-FeOOH appears much more on the plain carbon steel than the weathering steel. There is no special tendency in abundance of β-FeOOH in contrast to XRD from the rust layer surface. The depth range observed by XRD from the surface is only in the range of at most 2–3 μm from the surface. As shown in Fig. 1, XRD observation of the rust layer surface clearly shows high abundance of β-FeOOH on the skyward surface for every specimen. This may caused by the fact that the elements convoluted in the outermost region are different in quantity and species from other part (both inner layer and outer layer) of the rust layer. On the other hand, that of TEM/ED measurements of the cross section can cover whole the specimen rather than the surface region.

There is a view where the quantity ratio of α-FeOOH to β-FeOOH + γ-FeOOH + magnetite (α/γ^* ratio) detected by X ray diffraction can be used as an index for protection nature of a rust layer.[12, 13] Based on this view, the α/γ^* ratio was taken from TEM/ED observation. Without counting amorphous rust by TEM/ED to α-FeOOH, the α/γ^* ra-

tios were 1.51 and 1.15 for E19H-A (skyward) and E19H-B (earthward), respectively, and 0.97 and 0.74 for A19H-A (skyward) and A19H-B(earthward), respectively. On a weathering steel, the ratio $\alpha/\gamma^* > 1$, while that on a plain carbon steel, it is less than 1, and the α/γ^* value was larger on the skyward side than that on earthward side. It can be said that the α/γ^* ratio determined by ED seems to be good index for the protective nature of the rust layer. When amorphous rust by ED was counted as a part of α-FeOOH, every α/γ^* was more than 1.2, and it was largest on the earthward side of plain carbon steel. Although a part of XRD-amorphous rust was judged as crystalline in this work, there exists also still more amorphous rust even in TEM/ED observation. As mentioned above, however, the quatitative results can not be obtained for TEM/ED-amorphous rust because the intensity from TEM/ED-amorpous rust is not much clear. The α/γ^* ratio by TEM/ED will be applicable to the evaluation of rust layer without counting TEM/ED-amorphous rust.

4. Conclusions

Several weathering steels and a plain carbon steel exposed to atmosphere for 17 years at a coastal industrial region (Yokkaichi) and at a rural region (Mikuni Pass) with their faces being placed horizontally were investigated by EPMA, XRD, SEM and TEM/ED, and following conclusions were drawn:

(1)   Rust consists of three layer essentially; the inner, outer and outermost layers irrespective of a plain carbon steel or a weathering steel. The rust layer consists of α-FeOOH, β-FeOOH, γ-FeOOH, magnetite and amorphous rust.

(2)   The outermost layers is about 3 μm thick and enriched with atmospheric deposits. In the outer layer, Cl and S are enriched. Alloying elements, Cu, Cr and Si are concentrated in the inner layer while P and Ni is mostly distributed uniformly over the whole rust layer.

(3)   Irrespective of steels, the major component of the rust layer in the outermost layer is α-FeOOH and minors are β- and γ-FeOOH. β-FeOOH is especially abundant on the skyward surfaces.

(4)   In the outer and inner layers, the main constituent is α-FeOOH, which is formed more on skyward side than earthward side, and more on weathering steel than plain carbon steel. Abundance of γ-FeOOH is higher on the skyward rust layer than the earthward rust layer, and it exists more on a plain carbon steel. Magnetite appears more on the earthward side than on the skyward side, and more on a plain carbon steel than a weathering steel. There is no special tendency in abundance of β-FeOOH.

(5)   Silicon in the inner layer is in the forms of silicates.

(6)   The quantity ratio of α-FeOOH to β-FeOOH + γ-FeOOH + magnetite, the α/γ^* ratio, obtained by TEM/ED, is larger than 1 on a weathering steel, and less than 1 on a plain carbon steel. The TEM/ED determined α/γ^* value can be used as an index to evaluate the protective natutre of a rust layer as have been done with conventional XRD technique.

(7)   XRD and EPMA results shows almost no difference between specimens exposed at the industrial region (Site 19) and the rural region (Site 08) because of calcium chloride sprayed for melting snow on road during winter at Site 08.

REFERENCES

1) H. Okada, Y. Hosoi, K. Yukawa and H. Naito: Tetsu-to-Hagane (J. Iron and Steel Institute of Japan) **55** (1969) 355–365.
2) T. Misawa, M. Yamashita, Y. Matsuda, H. Miyuki and H. Nagano: Tetsu-to-Hagane (J. Iron and Steel Institute of Japan) **79** (1993) 69–75.
3) M. Yamashta, H. Miyuki, H. Nagano and T. Misawa: Zairyo-to-Kankyo (Corros. Eng.) **43** (1994) 26–32.
4) M. Yamamoto, H. Katayama and T. Kodama: Current advances in Materals and Processes (CAMP-ISIJ): **12** (1999) 422.
5) K. Shiotani, W. Tanimoto, C. Maeda, F. Kawabata and K. Amano: Zairyo-to-Kankyo (Corros. Eng.) **49** (2000) 67–71.
6) H. Kihira: *Electrochemical Phenomena at Interface*, ed. by H. Ohshima and K. Furukawa (Marcel Dekker, New York, 1998) pp. 429–440.
7) J. T. Keiser, C. W. Brown and R. H. Heidersbach: Corros. Sci. **23** (1983) 251–259.
8) M. Yamashita, K. Asami, T. Ishikawa, T. Ohtsuka, H. Tamura and T. Misawa: Zairyo-to-Kankyo (Corros. Eng.) **50** (2001) 521–530.
9) K. Asami: Trans., JIM **21** (1980) 302–308.
10) Private communication: Public Works Research Institute Ministry of Construction, Japan Association of Steel Bridge Construction and the Kozai Club.
11) M. Sakashita and N. Sato: Boshoku Gijutsu (Corros. Eng.) **28** (1979) 450–461.
12) M. Yamashita, H. Miyuki, Y. Matsuda, H. Nagano and T. Misawa: Corros. Sci. **36** (1994) 283–299.
13) H. Kihira, T. Misawa, T. Kusunoki, T. Tanabe and T. Saito: Zairyo-to-Kankyo (Corros. Eng.) **48** (1999) 727–732.